Supporting Information

Conditions for efficient charge generation preceded by energy transfer process in non-fullerene organic solar cells

L. Benatto,[a] C. A. M. Moraes,[a] G. Candiotto,[b] K. R. A. Sousa,[a] J. P. A. Souza,[a] L. S. Roman[a] and M. Koehler[a]

[a] Department of Physics, Federal University of Paraná, 81531-980, Curitiba-PR, Brazil

[b] Institute of Chemistry, Federal University of Rio de Janeiro, 21941-909, Rio de Janeiro-RJ, Brazil

Corresponding authors: lb08@fisica.ufpr.br, koehler@fisica.ufpr.br

S1. Molecular dynamics simulations

S1.1 The model

The mathematical model used to classically describe the dynamics of molecules is the model of all atoms. In this model, was used the force field composed of the potential

$$
\begin{aligned}
V \; = \; & \sum_{\text{bonds}} \frac{K_l}{2}(l_{ij} - l_0)^2 + \sum_{\text{angles}} \frac{K_\theta}{2}(\theta_{ijk} - \theta_0)^2 \; + \\
& + \sum_{\substack{\text{improper}\\\text{dihedrals}}} \frac{K_\xi}{2}(\xi_{ijkl} - \xi_0)^2 + \sum_{\substack{\text{proper}\\\text{dihedrals}}} \sum_{n=0}^{5} C_n[cos(\phi_{ijkl})]^n \; + \\
& + \sum_{j=1, j\neq i}^{N} 4\varepsilon_{ij}\left[\left(\frac{\sigma_{ij}}{r_{ij}}\right)^{12} - \left(\frac{\sigma_{ij}}{r_{ij}}\right)^{6}\right] + \sum_{j=1, j\neq i}^{N} \frac{q_i q_j}{4\pi\epsilon_0 r_{ij}} \; .
\end{aligned} \tag{S1}
$$

and parameters taken from the Optimized Potential for Liquid Simulations (OPLS) table.[1–3]

In Eq. (S1) the parameters l_0, θ_0, and ξ_0 represent, respectively, the equilibrium values of bond lengths, covalent angles, and improper dihedral angles. In these harmonic potentials, the $K_{l,\theta,\xi}$ parameters indicate their elastic constants. The fourth term is the Ryckaert-Bellemans potential,[4] which represents the torsion energy of a chain as a function of the φ_{ijkl} angle (proper dihedral angle); C_n parameters are coefficients taken from OPLS or studied via DFT. The last two terms represent the van der Waals (by Lennard-Jones equation) and electrostatic interactions, respectively. In these non-bonded interactions, the parameters ε_{ij} and σ_{ij} represent the characteristic energy and diameter between two particles i and j. The variable r_{ij} is the distance between such particles.

The values of the parameters present in the Lennard-Jones equation, for example, are shown in Table S1 and in the Table S2 is indicated in which molecules were used.

Table S1 - Parameters from the OPLS table used in the non-bonded interactions.

| Name	atom	mass [u]	σ_{ii} [nm]	ε_{ii} [kJ mol -1]
opls_236	O	15.9994	0.296	0.87864
opls_264	Cl	35.4530	0.340	1.25520
opls_567	C	12.0110	0.355	0.29288
opls_569	H	01.0080	0.242	0.12552
opls_633	S	32.0600	0.355	1.04600
opls_728	F	18.9984	0.285	0.25522
opls_900	N	14.0067	0.330	0.71128

1.2 Thin film production

Both solvent validation and solvent evaporation simulation were performed as in our previous work.[5,6] Partial atomic charges were obtained using the ESP formalism[7,8] and considering the acceptor molecules with the side groups.

The validation of the solvent was performed as follows: 200 molecules of chlorobenzene were added inside a box of dimensions (4.0×4.0×4.0) nm^3. In the sequence, was performed an energy minimization (with the steepest descent algorithm) to avoid overlapping particles; an molecular dynamics (MD) with the velocity-Verlet iteration algorithm in the NVT ensemble for 1.0 ns; an MD in the NPT ensemble for 1.0 ns with the Berendsen thermostat and 10.0 ns with the Nosé-Hoover thermostat. The resulting mass density was 1111.52±11.93 kg/m^3 at an average temperature of 300,016±5.01 K, as shown in Figure S1 (a). All simulations were performed with periodic boundary conditions (PBC) in the GROMACS package.[9]

We added 50 molecules for each molecule shown in Table S2 in a box with dimensions (9.0×9.0×9.0) nm^3 separately. Then, each box was filled with the previously thermalized chlorobenzene solvent (Figure 1 (b)), resulting in an average of 28215 atoms in each of the 10 systems. Subsequently, the size of this box was tripled on the *Z*-axis by adding two empty boxes above it for the eventual flow of solvent molecules.

Table S2 - Use of OPLS parameters (see Tab. 1) per molecule.

Materials	opls_236	opls_264	opls_567	opls_569	opls_633	opls_728	opls_900
IT-2F	✓	-	✓	✓	✓	✓	✓
IT-2Cl	✓	✓	✓	✓	✓	-	✓
IT-4F	✓	-	✓	✓	✓	✓	✓
IT-4Cl	✓	✓	✓	✓	✓	-	✓
ITCC	✓	-	✓	✓	✓	-	✓
IT-M	✓	-	✓	✓	✓	-	✓
ITIC	✓	-	✓	✓	✓	-	✓
IEICO	✓	-	-	✓	✓	-	✓
IEICO-4F	✓	-	✓	✓	✓	✓	✓
IEICO-4Cl	✓	✓	✓	✓	✓	-	✓
Chlorobenzene	-	✓	✓	✓	-	-	-
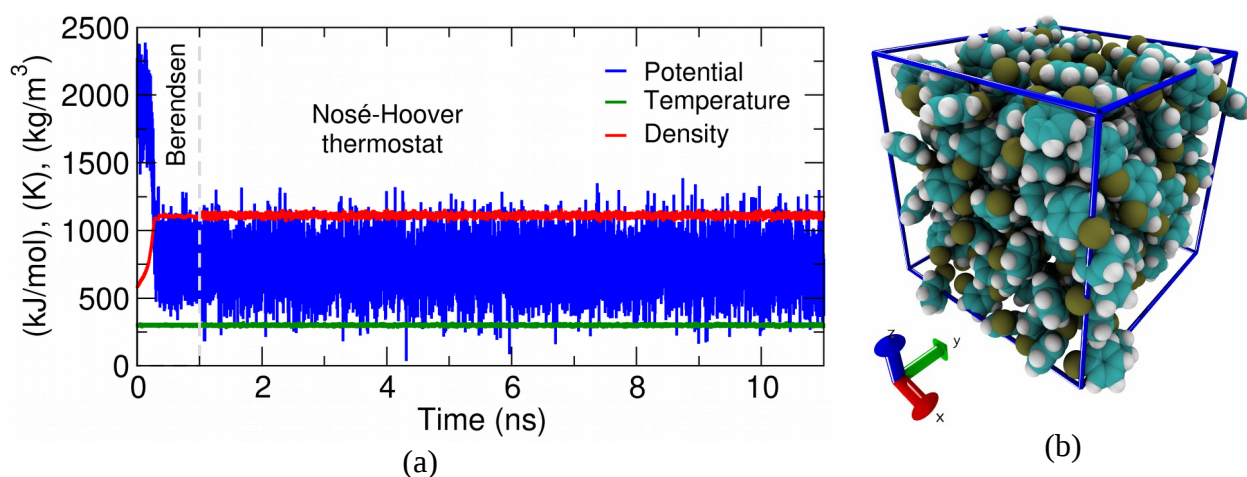
Figure S1 - (a) Time evolution of some thermodynamic properties during the use of Berendsen and Nosé-Hoover thermostats. (b) Snapshot of the box resulting from the validation of the chlorobenzene solvent.

The simulated solvent evaporation process had the following protocol: First, an energy minimization was performed. Then, two MDs were performed in the NVT ensemble: one for 1.0 ns using the Berendsen thermostat and one for 0.5 ns with the v-rescale thermostat. At the end of this simulation, 100 solvent molecules were removed, preferably those that were suspended in the volume above the material (in the gas-phase). If there were not enough molecules in the gas phase, molecules on the liquid's

surface (with a higher coordinate in *Z*) were removed. The last MD and consequent removal of molecules were repeated until all the solvent was removed, resulting in the thin films shown in Figure S2.
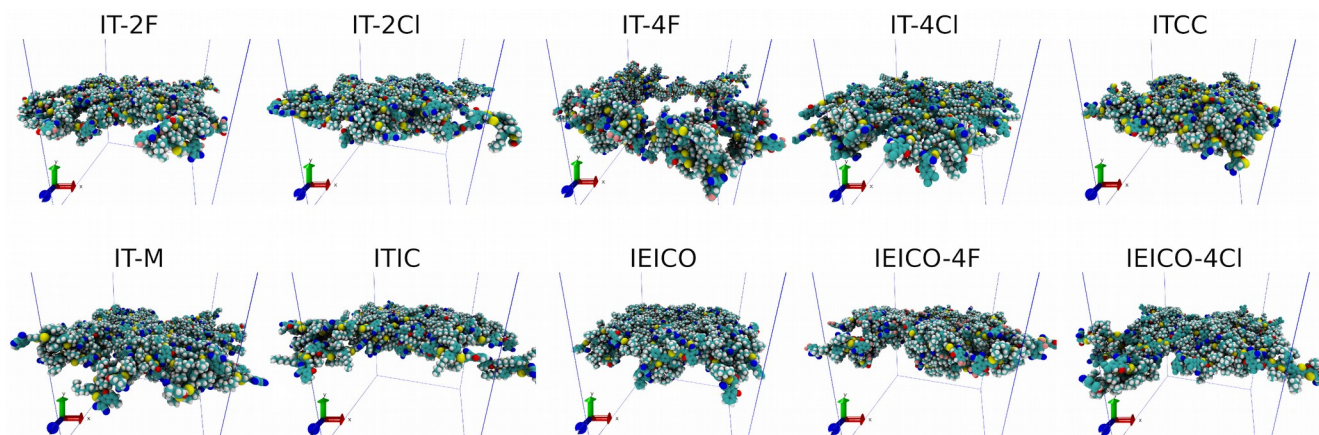
Figure S2 - Snapshots of thin films after 9.5 ns of MD at a temperature of 298.15 K in the NVT ensemble. Atoms are represented by the following colors: O = red; Cl = cyan; C = cyan (smaller sphere); H = white; S = yellow; F = pink and N = blue.

1.3 Molecular volume

The molecular volume was calculated by obtaining the Fractional Free Volume (FFV)[10] calculated by Gromacs.[11] FFV is related to Free Volume (FV) through

$$FFV = 1.3 \cdot FV - 0.3.$$ (S2)

Then, the molecular volume can be obtained through the following expression:

$$\langle Molecular\ volume \rangle = \frac{(1.0 - FFV) \cdot V}{N},$$ (S3)

where *V* is the real volume of the simulation box and *N* the number of molecules within this volume.

S2. Modification of quenching expressions considering FRET

We start from the hypothesis that there is an average number of N excited donor molecules near an acceptor. In an interval dt, n_1 of those N molecules can transfer the electron to the acceptor and produce a CT state (group 1). Alternatively, n_2 of those donors can either transfer its energy by FRET to the acceptor (donor-acceptor FRET) or transfer the electron to form a CT exciton (group 2). From the above assumptions $n_1 + n_2 = N$. The time variation of the singlet state, $[S_{1,D}]$, in group 1 (defined in ref.[12]) is

$$\frac{d[S_{1,D}]}{dt} = I - k_{SR,D}[S_{1,D}] - k_{ET}[S_{1,D}] + k_{EB}[CT], \tag{S4}$$

where, I is the rate of exciton generation in the donor at the D/A interface that involves the source of excitons produced by photon absorption or the net flow of excitons transferred by FRET from (to) other donors (at a rate $k_{F,DD}$). $k_{SR,D}$ in Eq. (S4) is the donor singlet exciton recombination rate (the inverse of singlet exciton recombination lifetime), [CT] is the concentration of CT state, k_{ET} is the electron transfer rate from $S_{1,D}$ to CT, k_{ET} is the electron back rate from CT to $S_{1,D}$.

Using the above assumptions, the time variation of the singlet state concentration in group 2 of donors is

$$\frac{d[S_{1,D}]}{dt} = I - k_{SR,D}[S_{1,D}] - k_{ET}[S_{1,D}] + k_{EB}[CT] - k_{F,DA}[S_{1,D}], \tag{S5}$$

where $k_{F,DA}$ is the FRET rate from the donor to acceptor. The total variation of the singlet state in the N molecules is given by adding Eqs. (S4) and (S5) or

$$\frac{d[S_{1,D}]}{dt} = -\frac{n_2}{N}k_{F,DA}[S_{1,D}] + c, \tag{S6}$$

where $c \equiv I - k_{SR,D}[S_{1,D}] - k_{ET}[S_{1,D}] + k_{EB}[CT]$. If N is sufficiently high, the probability that one excited donor will belong to group 2 is $p_{F,DA} \approx n_2 / N$. Hence Eq. (S6) can be given as a function of $p_{F,DA}$

$$\frac{d[S_{1,D}]}{dt}=-p_{F,DA}k_{F,DA}[S_{1,D}]+c. \tag{S7}$$

Upon charge transfer, the time-dependent concentration of CT state at the D/A heterojunction is related to $[S_{1,D}]$ by

$$\frac{d[CT]}{dt}=k_{ET}[S_{1,D}]-k_{EB}[CT]-k_{ER}[CT]-k_{ES}[CT], \tag{S8}$$

where k_{ER} is the electron recombination rate from CT to the ground state and k_{ES} is the rate of CT dissociation by electron separation. Due to small oscillation strength associated to the CT state, here we are neglecting the contribution to [CT] of states formed by direct light absorption.

Under the steady state approximation, Eq. (S7) and (S8) gives

$$I=k_{SR,D}[S_{1,D}]+k_{ET}[S_{1,D}]-k_{EB}[CT]+p_{F,DA}k_{F,DA}[S_{1,D}], \tag{S9}$$

$$[CT]=\frac{k_{ET}[S_{1,D}]}{k_{EB}+k_{ER}+k_{ES}} \tag{S10}$$

Substituting Eq. (S10) in (S9) one finds

$$[S_{1,D}]=f_D I, \tag{S11}$$

where

$$f_D=\frac{k_{EB}+k_{ER}+k_{ES}}{(k_{SR,D}+k_{ET}+p_{F,DA}k_{F,DA})(k_{EB}+k_{ER}+k_{ES})-k_{EB}k_{ET}} \tag{S12}$$

After the donor-acceptor FRET, the exciton at the acceptor can either recombine emitting a photon or be dissociated by hole transfer to the donor. Hence, the population of excitons in the acceptor also influences the quenching even for selective illumination of the donor due to the D-A FRET. Using the same reasoning and steps followed to find Eq. (S11), one can analogously write the population of (FRET induced) singlet excitons

in the acceptor $[S_{1,A}]_F$ as

$$[S_{1,A}]_F = f_A k_{F,DA}[S_{1,D}] = f_A k_{F,DA} f_D I, \tag{S13}$$

where

$$f_A = \frac{k_{HB} + k_{HR} + k_{HS}}{(k_{A,SR} + k_{HT})(k_{HB} + k_{HR} + k_{HS}) - k_{HB} k_{HT}}. \tag{S14}$$

In Eq. (S13), it is already assumed that the energy transfer between the acceptor and donor is absent so that $k_{F,AD} = 0$.

In the absence of the acceptor (hence considering only an isolated donors), the time variation of the singlet state concentration $[S'_{1,D}]$ at the same position of the concentration given by Eq. (S11), would be given by

$$\frac{d[S'_{1,D}]}{dt} = I' - k_{SR,D}[S'_{1,D}], \tag{S15}$$

where I' is the rate of exciton generation in the absence of the acceptor.

From Eq. (S15) assuming steady state conditions,

$$I' = k_{SR,D}[S'_{1,D}] \tag{S16}$$

or

$$[S'_{1,D}] = \frac{I'}{k_{SR,D}}. \tag{S17}$$

We define the exciton quenching as

$$Q_D = 1 - \left(\frac{(1 - p_{F,DA})[S_{1,D}] + p_{F,DA}[S_{1,A}]_F}{[S'_{1,D}]} \right)$$

$$Q_D = 1 - \left(\frac{(1 - p_{F,DA})[S_{1,D}] + p_{F,DA} f_A k_{F,DA}[S_{1,D}]}{[S'_{1,D}]} \right). \tag{S18}$$

If the acceptor is inefficient to quench the excitons and assuming $I \approx I'$, then $[S'_{1,D}] \approx (1 - p_{F,DA})[S_{1,D}] + p_{F,DA}[S_{1,A}]_F$ from energy conservation Eq. (S18) then gives $Q_D \approx 0$. Alternatively, if the acceptor is efficient to dissociate the excitons induce in the

donor, then $[S_{1,D}] \approx 0$ and from Eq. (S18) $Q_D \approx 1$. Note that the D-A FRET is not dominant when $p_{F,DA} \approx 0$ so that the exciton quenching is determined mainly by the electron transfer from the donor to the acceptor. On the other hand, if $p_{F,DA} \approx 1$, the exciton quenching will be determined by a multiple step process that involves the donor-acceptor FRET and the following transfer of holes to the donor. Using Eqs. (S13) and (S17), after a few manipulations of the equations above one gets

$$Q_D = 1 - k_{SR,D} f_D \big((1 - p_{F,DA}) + p_{F,DA} k_{F,DA} f_A \big). \tag{S19}$$

The quenching dynamics described by Eq. (S19) will be completely determined once the probability $p_{F,DA}$ is known. We will assume that $p_{F,DA}$ depends on the process that deactivates (or reactivates) the singlet donor state.[13] This probability will also depend on the average density of donor (n_D) or acceptor (n_A) molecules surrounding a determined excited donor that are available to receive the exciton, i.e. the number of acceptors per donor (n_D/n_A).[13] For a homogeneous blend (in which donor and acceptor have a similar average density) $n_A/n_D \approx 1$. Additionally, the D/A ratio of the ten blends considered in this work is 1:1 (weight by weight, w/w).[14] Under those assumptions $p_{F,DA}$ will depend on the $k_{F,DD}$, $k_{SR,D}$, k_{ET} and k_{EB} in the form:

$$p_{F,DA} = \frac{k_{F,DA}}{k_{F,DA} + k_{F,DD} + k_{SR,D} + k_{ET} - k_{EB}}. \tag{S20}$$

For example, when k_{ET} (or $k_{F,DD}$) is much higher than $k_{F,DA}$ (combined with a negligible k_{EB}), $p_{F,DA} \approx 0$ and exciton quenching is produced almost exclusively by electron transfer from the donor to the acceptor. In this case, the expression for Q_D in Eq. (S19) is reduced to the formula proposed in ref.[12] (deduced without considering the FRET between donor and acceptor).

Finally, considering the selective excitation of the acceptor, we can repeat the same reasoning above to calculate Q_A. By assuming now that the quenching is produced only by a hole transfer to the donor ($k_{F,AD} = 0$), one finds:

$$Q_A = 1 - \frac{[S_{1,A}]}{[S_{1,A}']} = 1 - k_{SR,A} f_A. \tag{S21}$$

S3. FRET rates

In FRET model, the FRET rate k_F between donor and acceptor is given by ref[15]

$$k_F = \frac{1}{\tau_D}\left(\frac{R_0}{R}\right)^6 \tag{S22}$$

where τ_D is the exciton lifetime of the donor in the absence of the acceptor (equal to 178 ps for PBDB-TF[16]), R_0 is the Förster radius, and R is the donor-acceptor distance. R_0 corresponds to a separation distance at which the rate of transfer matches the rate of exciton decay: $k_{FRET} = \tau_D^{-1}$. In nanometer, R_0 can be expressed as

$$R_0 = 0.0211\left(\frac{\kappa^2\,\Theta_D\,J(\lambda)}{n^4}\right)^{\frac{1}{6}} \tag{S23}$$

where κ^2 is the dipole-dipole orientation factor (set equal to 2/3 that correspond to a random relative orientation of the molecular dipoles), n is the refraction index of the medium, Θ_D is the quantum yield of the donor fluorescence in the absence of the acceptor (equal to 1.26 % for PBDB-TF[16]), and J is the overlap integral between the acceptor absorption spectrum and the normalized emission spectrum of the donor. The dipole approximation breaks down at shorter D−A distances.[17]

We use the Kramers-Kronig relation to obtain the refractive index n following the procedure described in detail in ref.[18]. For the procedure, the absorption coefficient of each blend is required. In Figure S3 and Figure S4 the absorption coefficient of each blend and the calculated refractive index are presented. Karuthedath et al.[16] argued that the Kramers-Kronig relation approximates the refractive indexes very well, with a few percentage of deviation in relation of ellipsometry measurements. With the results of Figure S6, we obtained the effective refractive index n_{efl}, that is computed as a weighted average of n(λ), weighted for the amplitude of the overlap between the donor's emission and the acceptor's absorption.[16]
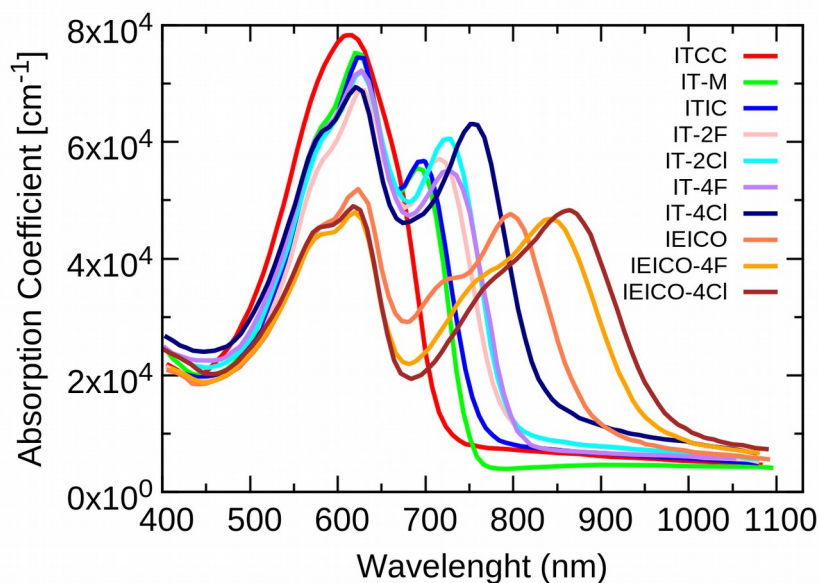
Figure S3 - Absorption coefficient of the PBDB-TF-based blend films. Experimental results of ref.[13].
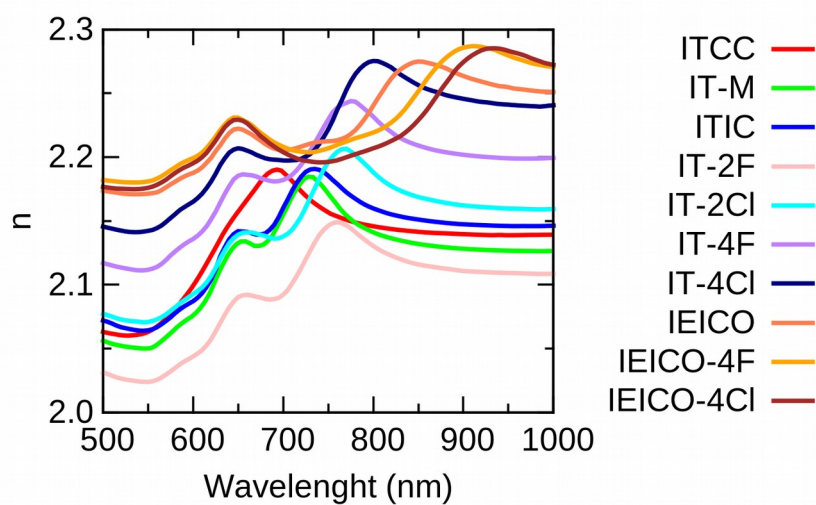
**Figure S4** - Refractive index of the blend films determined using the Kramers Kronig relation.

For calculating J, the acceptor absorption spectrum and the emission spectrum of the donor are presented in Figure S5. The overlap region for each blend is highlighted in Figure S6. $J(\lambda)$ can be calculated in units of mol^{-1} L cm^{-1} nm^4 using the formula:[16]

$$J(\lambda)=\int_0^\infty \varepsilon_A(\lambda)\lambda^4 F_D(\lambda)d\lambda \qquad\qquad (S24)$$

where $\varepsilon_A(\lambda)$ is the molar extinction (attenuation) coefficient of the acceptor in units of mol^{-1} cm^{-1} and $F_D(\lambda)$ is the wavelength-dependent donor emission spectrum normalized to its area.[13] To obtain $\varepsilon_A(\lambda)$ it is necessary to know the films' absorption coefficients α, molecular weight M_w, and the density d of materials (a typical value of d for polymeric materials is 1.2 kg/L[19]):

$$\varepsilon_A(\lambda)=\frac{\alpha(\lambda)M_W}{d}. \qquad\qquad (S25)$$

The input parameters to obtain k_F are presented in Table S3.
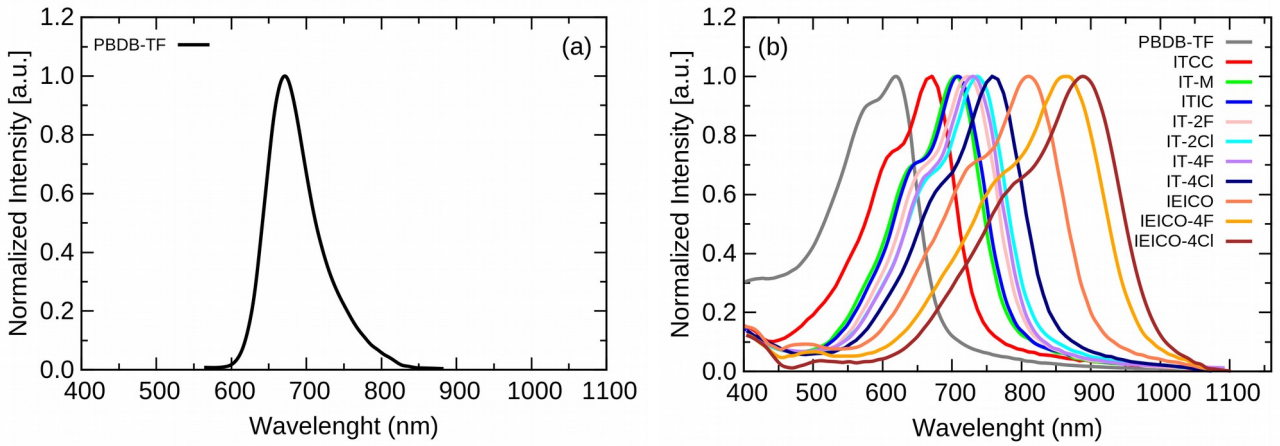
Figure S5 – (a) Photoluminescence spectra of neat PBDB-TF film. (b) UV-vis absorption spectra of the neat films. Experimental results of ref[14].
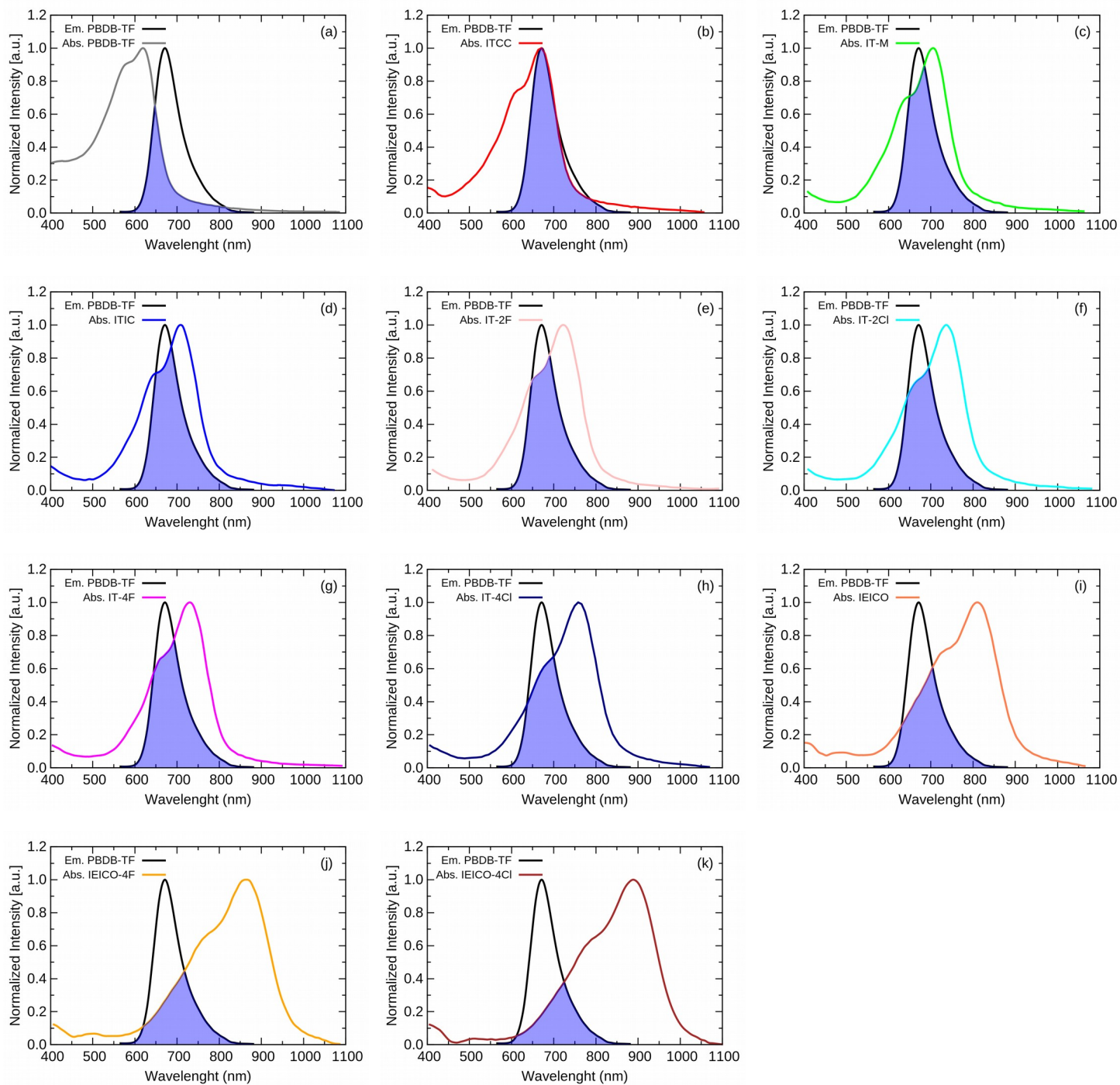
Figure S6 - Overlap (highlighted blue region) between the PBDB-TF emission and NFA absorption spectra. Experimental results of ref[14].

Table S3 - Input parameters and results of k_F.

Blends	$M_{w,A}$ (g/mol)	n_{eff}	$J(\lambda)$ (mol^{-1} L cm^{-1} nm^{-4})	R_0 (nm)	R^{a} (nm)	k_F (s^{-1})	$p_{F,DA}{}^{b}$ (%)
D/IT-2F	1464	2.10	2.18×10^{16}	3.06	1.0	4.63×10^{12}	44.6
D/IT-2Cl	1497	2.15	2.16×10^{16}	3.01	0.9	7.84×10^{12}	61.2
D/IT-4F	1500	2.19	2.19×10^{16}	2.98	0.9	7.38×10^{12}	59.7
D/IT-4Cl	1566	2.21	2.11×10^{16}	2.94	0.9	6.88×10^{12}	67.5
D/ITCC	1437	2.17	2.18×10^{16}	2.99	0.9	7.63×10^{12}	30.3
D/IT-M	1456	2.15	2.23×10^{16}	3.03	0.9	8.11×10^{12}	38.6
D/ITIC	1428	2.16	2.17×10^{16}	3.00	0.9	7.72×10^{12}	43.7
D/IEICO	1736	2.21	2.10×10^{16}	2.94	1.3	7.51×10^{11}	9.1
D/IEICO-4F	1808	2.21	1.73×10^{16}	2.85	1.6	1.78×10^{11}	4.9
D/IEICO-4Cl	1874	2.20	1.53×10^{16}	2.80	1.7	1.12×10^{11}	3.3
D/D	1250^{c}	2.32^{d}	0.79×10^{16}	2.42	0.9	2.12×10^{12}	-

^{a} Value from 0.9 nm that best correlated Q_D–Theo. with Q_D–Exp.. ^{b} Calculated using equation (S20).
^{c} Molecular weight of the monomer unit. ^{d} From $n(\lambda)$ determined by ellipsometry by ref.[16].

S4. Complementary results

Table S4 - Energy of charge transfer state. Results in eV.

Blends	Ref.[16]	Ref.[14]
	$E_{CT}{}^{a}$	$E_{CT} = E_{LUMO,A} - E_{HOMO,D}{}^{b}$
D/IT-2F	-	1.49
D/IT-2Cl	-	1.46
D/IT-4F	1.50	1.45
D/IT-4Cl	-	1.40
D/ITCC	-	1.66
D/IT-M	-	1.58
D/ITIC	-	1.55
D/IEICO	1.49	1.58
D/IEICO-4F	1.42	1.44
D/IEICO-4Cl	-	1.40

^{a}Obtained from electroluminescence spectra of blends. ^{b}The molecular energy levels of the materials were measured by cyclic voltammetry (CV).

Table S5 - Optimal range-separation parameter, ω (Bohr^{-1}), ionization potential, IP, electron affinity, EA, fundamental gap, E_{fund}, optical gap, E_{opt} and exciton binding energy, E_b^{vac} (all the energies in eV).

Materials	ω	IP	EA	E_{fund}	E_{opt}	E_b^{vac}
IT-2F	0.0860	6.362	2.410	3.953	2.117	1.836
IT-2Cl	0.0850	6.390	2.461	3.929	2.108	1.821
IT-4F	0.0860	6.431	2.474	3.957	2.120	1.837
IT-4Cl	0.0830	6.456	2.575	3.880	2.081	1.800
ITCC	0.0890	6.324	2.040	4.284	2.339	1.945
IT-M	0.0861	6.237	2.249	3.989	2.146	1.843
ITIC	0.0861	6.297	2.303	3.993	2.144	1.850
IEICO	0.0810	5.783	2.258	3.525	1.831	1.694
IEICO-4F	0.0811	5.904	2.422	3.482	1.806	1.676
IEICO-4Cl	0.0799	5.935	2.517	3.418	1.775	1.644
PBDB-TF	0.0890	5.854	1.561	4.294	2.284	2.009

Table S6 - Intramolecular reorganization energies derived at the tuned ωB97XD/6-31g(d,p) levels. Results in eV.

Materials	Electron		Hole	
	λ_e^{A-A}	λ_e^{D-A}	λ_h^{D-D}	λ_h^{A-D}
IT-2F	0.284	0.321	-	0.309
IT-2Cl	0.287	0.322	-	0.310
IT-4F	0.297	0.327	-	0.315
IT-4Cl	0.280	0.319	-	0.307
ITCC	0.329	0.345	-	0.330
IT-M	0.230	0.329	-	0.317
ITIC	0.296	0.327	-	0.315
IEICO	0.259	0.309	-	0.296
IEICO-4F	0.261	0.309	-	0.297
IEICO-4Cl	0.249	0.303	-	0.291
PBDB-TF	-	-	0.346	-

Table S7 - Parameters and results of the driving force for charge transfer. Results in eV.

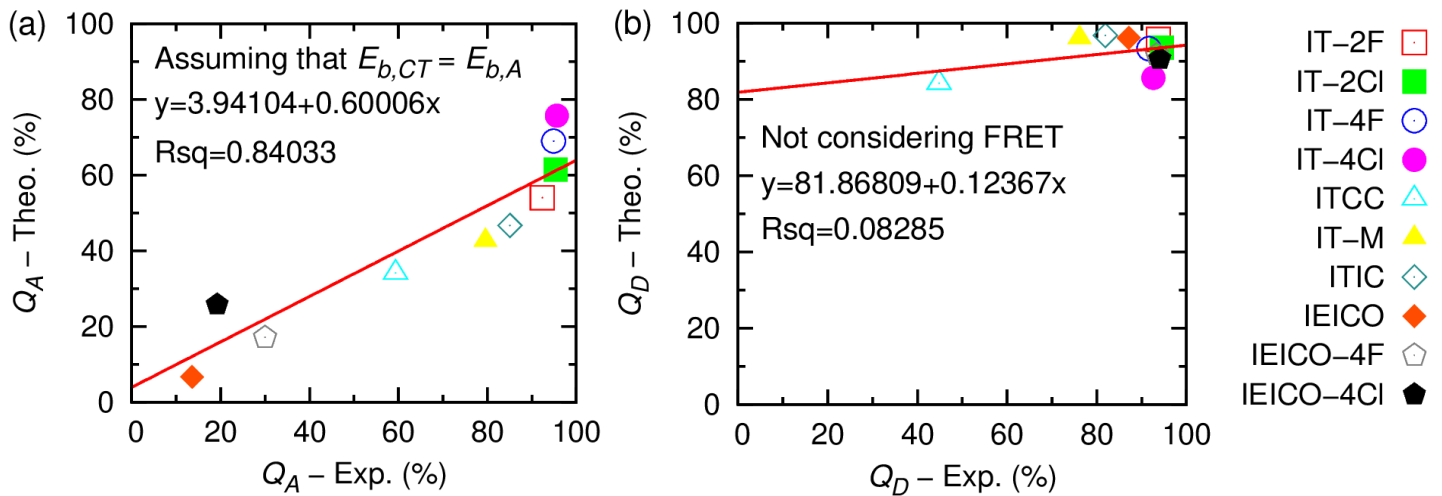| Blends	ΔE_{LUMO}[a]	$E_{b,D}$	ΔE_{HOMO}[a]	$E_{b,A}$	$E_{b,CT}$	$\Delta G_{ET} = \Delta E_{LUMO} - (E_{b,D} - E_{b,CT})$	$\Delta G_{HI} = \Delta E_{HOMO} - (E_{b,A} - E_{b,CT})$
D/IT-2F	−0.39	0.50	−0.21	0.42	0.32	−0.57	−0.31
D/IT-2Cl	−0.42	0.50	−0.22	0.40	0.30	−0.62	−0.32
D/IT-4F	−0.43	0.50	−0.24	0.39	0.30	−0.63	−0.33
D/IT-4Cl	−0.48	0.50	−0.25	0.37	0.29	−0.69	−0.33
D/ITCC	−0.22	0.50	−0.15	0.43	0.38	−0.34	−0.20
D/IT-M	−0.30	0.50	−0.16	0.41	0.34	−0.46	−0.23
D/ITIC	−0.33	0.50	−0.18	0.41	0.33	−0.50	−0.26
D/IEICO	−0.30	0.50	0.10	0.34	0.32	−0.48	0.08
D/IEICO-4F	−0.44	0.50	0.02	0.34	0.32	−0.62	0.00
D/IEICO-4Cl	−0.48	0.50	−0.01	0.33	0.36	−0.62	0.02

[a]The molecular energy levels of the materials were measured by cyclic voltammetry (CV).[14]

**Table S8** - Driving forces (eV) and Marcus rates (s^{-1}) for electron dynamics.

Blends	ΔG_{ET}	k_{ET} (λ_e^{D-A})	ΔG_{EB}	k_{EB} (λ_e^{D-A})	ΔG_{ER}	k_{ER} (λ_e^{D-A})	ΔG_{ES}	k_{ES} (λ_e^{A-A})
D/IT-2F	−0.57	9.75 x 10^{12}	0.57	9.52 x 10^{6}	−1.17	5.36 x 10^{7}	0.32	2.00 x 10^{10}
D/IT-2Cl	−0.62	5.14 x 10^{12}	0.62	1.92 x 10^{6}	−1.14	1.07 x 10^{8}	0.30	2.99 x 10^{10}
D/IT-4F	−0.63	5.48 x10^{12}	0.63	8.85 x 10^{5}	−1.12	2.22 x 10^{8}	0.30	2.70 x 10^{10}
D/IT-4Cl	−0.69	2.00 x 10^{12}	0.69	7.37 x 10^{4}	−1.08	5.36 x 10^{8}	0.29	4.30 x 10^{10}
D/ITCC	−0.34	3.19 x 10^{13}	0.34	5.94 x 10^{9}	−1.32	1.39 x 10^{6}	0.38	3.12 x 10^{9}
D/IT-M	−0.46	2.05 x 10^{13}	0.46	2.80 x 10^{8}	−1.25	3.59 x 10^{6}	0.34	1.05 x 10^{10}
D/ITIC	−0.50	1.62 x10^{13}	0.50	7.53 x 10^{7}	−1.22	8.79 x 10^{6}	0.33	1.46 x 10^{10}
D/IEICO	−0.48	1.58 x 10^{13}	0.48	1.75 x 10^{8}	−1.27	3.78 x 10^{5}	0.32	2.46 x 10^{10}
D/IEICO-4F	−0.62	4.56 x 10^{12}	0.62	2.37 x 10^{6}	−1.13	5.88 x 10^{7}	0.32	2.43 x 10^{10}
D/IEICO-4Cl	−0.62	3.77 x 10^{12}	0.62	1.42 x 10^{6}	−1.10	1.40 x 10^{8}	0.36	1.19 x 10^{10}

Table S9 - Driving forces (eV) and Marcus rates (s^{-1}) for hole dynamics.

Blends	ΔG_{HT}	k_{HT} (λ_h^{A-D})	ΔG_{HB}	k_{HB} (λ_h^{A-D})	ΔG_{HR}	k_{HR} (λ_h^{A-D})	ΔG_{HS}	k_{HS} (λ_h^{D-D})
D/IT-2F	–0.31	2.94 x 10^{13}	0.31	1.66 x 10^{10}	–1.17	1.72 x 10^7	0.32	9.89 x 10^9
D/IT-2Cl	–0.32	2.95 x 10^{13}	0.32	1.65 x 10^{10}	–1.14	4.09 x 10^7	0.30	1.71 x 10^{10}
D/IT-4F	–0.33	2.93 x 10^{13}	0.33	1.08 x 10^{10}	–1.12	7.50 x 10^7	0.30	1.54 x 10^{10}
D/IT-4Cl	–0.33	2.94 x 10^{13}	0.33	1.23 x 10^{10}	–1.08	2.30 x 10^8	0.29	2.31 x 10^{10}
D/ITCC	–0.20	2.14 x 10^{13}	0.20	1.43 x 10^{11}	–1.32	2.72 x 10^5	0.38	2.38 x 10^9
D/IT-M	–0.23	2.56 x 10^{13}	0.23	9.80 x 10^{10}	–1.25	1.01 x 10^6	0.34	6.77 x 10^9
D/ITIC	–0.26	2.75 x 10^{13}	0.26	5.65 x 10^{10}	–1.22	2.65 x 10^6	0.33	8.89 x 10^9
D/IEICO	0.08	1.88 x 10^{12}	–0.08	1.21 x 10^{13}	–1.27	8.60 x 10^4	0.32	1.07 x 10^{10}
D/IEICO-4F	0.00	5.00 x 10^{12}	0.00	5.46 x 10^{12}	–1.13	1.84 x 10^7	0.32	1.01 x 10^{10}
D/IEICO-4Cl	0.02	4.38 x 10^{12}	–0.02	7.38 x 10^{12}	–1.10	5.46 x 10^7	0.36	5.00 x 10^9

Figure S7 - Correlation between theoretical and experimental results of quenching efficiency for the PBDB-TF-based blends. (a) Q_A was calculated assuming that $E_{b,CT} = E_{b,A}$. (b) Q_D was calculated from equation 3 considering $p_{FRET,DA} = 0$. The linear equation and the R_{sq} are displayed in detail.
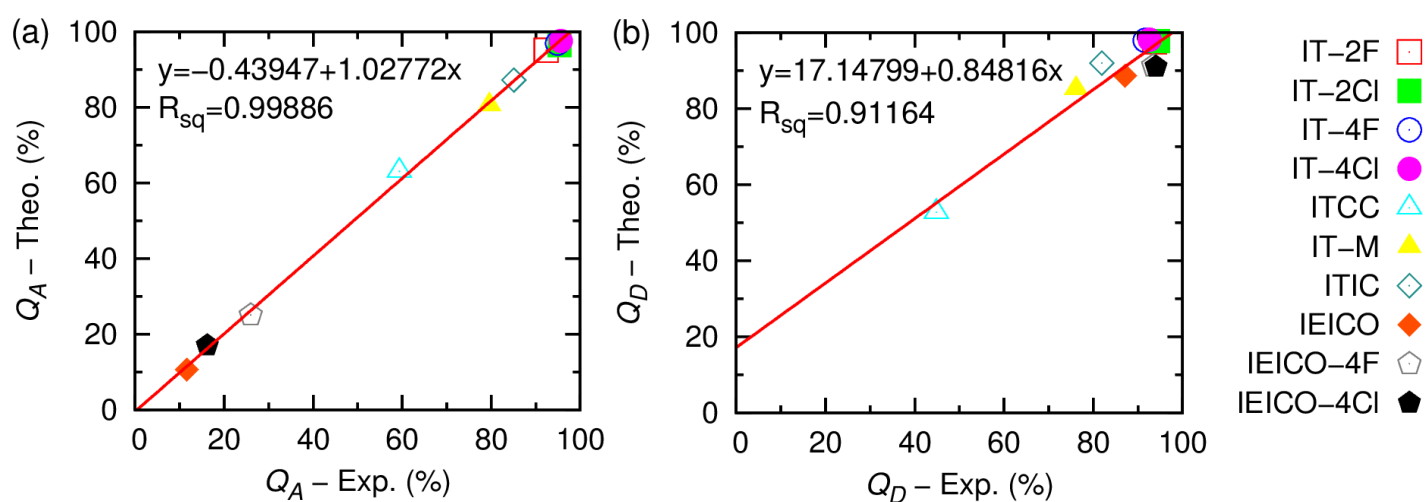
Figure S8 - Correlation between theoretical and experimental results of (a) Q_A and (b) Q_D for the PBDB-TF-based blends. For these results we have replaced the non-radiative recombination rate *via* CT calculated from the Marcus-Hush model by the data presented in ref.[20] calculated from the Marcus–Levich–Jortner model. The linear equation and the R_{sq} are displayed in detail.
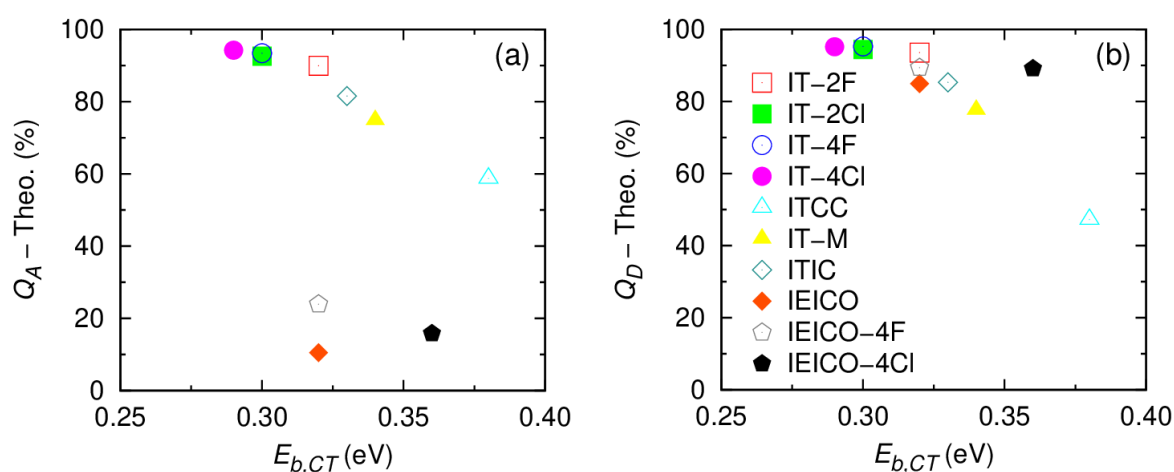
Figure S9 – (a) Q_D – Theo. and (b) Q_A – Theo. as a function of $E_{b,CT}$.

S5. References

(1)   Jorgensen, W. L.; Maxwell, D. S.; Tirado-Rives, J. Development and Testing of the OPLS All-Atom Force Field on Conformational Energetics and Properties of Organic Liquids. *J. Am. Chem. Soc* **1996**, *118* (45), 11225–11236.

(2)   Jorgensen, W. L.; Binning Jr, R. C.; Bigot, B. Structures and Properties of Organic Liquids: N-Butane and 1,2-Dichloroethane and Their Conformation Equilibriums. *J. Am. Chem. Soc.* **1981**, *103* (15), 4393–4399.

(3)   Kaminski, G. A.; Friesner, R. A.; Tirado-rives, J.; Jorgensen, W. L. Evaluation and Reparametrization of the OPLS-AA Force Field for Proteins via Comparison with Accurate Quantum Chemical Calculations on Peptides. *J. Phys. Chem. B* **2001**, *105*, 6474–6487.

(4)   Ryckaert, J.-P.; Bellemans, A. Molecular Dynamics of Liquid N-Butane near Its Boiling Point. *Chem. Phys. Lett.* **1975**, *30* (1), 123–125.

(5)   Sousa, K. R. A.; Benatto, L.; Wouk, L.; Roman, L. S.; Koehler, M. Effects of Non-Halogenated Solvent on the Main Properties of a Solution-Processed Polymeric Thin Film for Photovoltaic Applications: A Computational Study. *Phys. Chem. Chem. Phys.* **2020**, *22*, 9693–9702.

(6)   Benatto, L.; Sousa, K. R. A.; Koehler, M. Driving Force for Exciton Dissociation in Organic Solar Cells: The Influence of Donor and Acceptor Relative Orientation. *J. Phys. Chem. C* **2020**, *124* (25), 13580–13591.

(7)   Cox, S. R.; Williams, D. E. Representation of the Molecular Electrostatic Potential by a Net Atomic Charge Model. *J. Comput. Chem.* **1981**, *2* (3), 304–323.

(8)   Singh, U. C.; Kollman, P. A. An Approach to Computing Electrostatic Charges for Molecules. *J. Comput. Chem.* **1984**, *5* (2), 129–145.

(9)   Abraham, M. J.; Murtola, T.; Schulz, R.; Páll, S.; Smith, J. C.; Hess, B.; Lindah, E. Gromacs: High Performance Molecular Simulations through Multi-Level Parallelism from Laptops to Supercomputers. *SoftwareX* **2015**, *1–2*, 19–25.

(10)   Lee, W. M. Selection of Barrier Materials From Molecular Structure. *Polym. Eng. Sci.* **1980**, *20* (1), 65–69.

(11)   Lourenço, T. C.; Coelho, M. F. C.; Ramalho, T. C.; Van Der Spoel, D.; Costa, L. T. Insights on the Solubility of CO2 in 1-Ethyl-3-Methylimidazolium Bis(Trifluoromethylsulfonyl)Imide from the Microscopic Point of View. *Environ. Sci. Technol.* **2013**, *47* (13), 7421–7429.

(12)   Benatto, L.; Bassi, M. de J.; Menezes, L. C. W. de; Roman, L. S.; Koehler, M.

Kinetic Model for Photoluminescence Quenching by Selective Excitation of D/A Blends: Implications for Charge Separation in Fullerene and Non-Fullerene Organic Solar Cells. *J. Mater. Chem. C* **2020**, *8* (26), 8755–8769.

(13)   Chou, K. F.; Dennis, A. M. Förster Resonance Energy Transfer between Quantum Dot Donors and Quantum Dot Acceptors. *Sensors (Switzerland)* **2015**, *15* (6), 13288–13325.

(14)   Yang, C.; Zhang, J.; Liang, N.; Yao, H.; Wei, Z.; He, C.; Yuan, X.; Hou, J. Effects of Energy-Level Offset between a Donor and Acceptor on the Photovoltaic Performance of Non-Fullerene Organic Solar Cells. *J. Mater. Chem. A* **2019**, *7* (32), 18889–18897.

(15)   Clapp, A. R.; Medintz, I. L.; Mauro, J. M.; Fisher, B. R.; Bawendi, M. G.; Mattoussi, H. Fluorescence Resonance Energy Transfer between Quantum Dot Donors and Dye-Labeled Protein Acceptors. *J. Am. Chem. Soc.* **2004**, *126* (1), 301–310.

(16)   Karuthedath, S.; Gorenflot, J.; Firdaus, Y.; Chaturvedi, N.; Castro, C. S. P. De; Harrison, G. T.; Khan, J. I.; Markina, A.; Balawi, A. H.; Archie, T.; et al. Intrinsic Efficiency Limits in Low-Bandgap Non-Fullerene Acceptor Organic Solar Cells. *Nat. Mater.* **2021**, *20*, 378–384.

(17)   Ostroverkhova, O. Organic Optoelectronic Materials: Mechanisms and Applications. *Chem. Rev.* **2016**, *116* (22), 13279–13412.

(18)   Balawi, A. H.; Kan, Z.; Gorenflot, J.; Guarracino, P.; Chaturvedi, N.; Privitera, A.; Liu, S.; Gao, Y.; Franco, L.; Beaujuge, P.; et al. Quantification of Photophysical Processes in All-Polymer Bulk Heterojunction Solar Cells. *Sol. RRL* **2020**, *4* (6), 1–10.

(19)   Density of Plastics Material: Technical Properties Table. Available at Https://Omnexus.Specialchem.Com/Polymer-Properties/Properties/Density#values. (Accessed 31 May 2021).

(20)   Chen, X. K.; Qian, D.; Wang, Y.; Kirchartz, T.; Tress, W.; Yao, H.; Yuan, J.; Hülsbeck, M.; Zhang, M.; Zou, Y.; et al. A Unified Description of Non-Radiative Voltage Losses in Organic Solar Cells. *Nat. Energy* **2021**.